Measurements of atmospheric ethene by solar absorption FTIR spectrometry

Geoffrey C. Toon, Jean-Francois L. Blavier, Keeyoon Sung
Jet Propulsion Laboratory, California Institute of Technology, CA 91109, USA

5   *Correspondence to:* Geoffrey.C.Toon@jpl.nasa.gov

Abstract. Atmospheric ethene (C_2H_4; ethylene) amounts have been retrieved from high-resolution solar absorption spectra measured by the Jet Propulsion Laboratory (JPL) MkIV interferometer. Data recorded from 1985 to 2016 from a dozen ground-based sites have been analyzed, mostly between 30°N and 67°N. At clean-air sites such as Alaska, Sweden, New

10   Mexico, or the mountains of California, the ethene columns were always less than 1×10^{15} molec.cm^{-2} and therefore undetectable. In urban sites such as JPL, California, ethene was measurable with column amounts of 20×10^{15} molec.cm^{-2} observed in the 1990s. Despite the increasing population and traffic in Southern California, a factor 3 decrease in ethene column density is observed over JPL in the past 25 years, accompanied by a decrease in CO. This is

15   likely due to Southern California's increasingly stringent vehicle exhaust regulations and tighter enforcement over this period.

1 Introduction

Atmospheric ethene arises from microbial activity in soil and water, biological formation in plants, and by incomplete combustion from sources such as biomass burning, power plants,

20   and combustion engines. Ethene is primarily destroyed by reaction with OH (Olivella and Sole, 2004), which is rapid, giving ethene a tropospheric lifetime of only 1 to 3 days. Despite covering only 29% of the Earth's area, the land produces 89% of the ethene (Sawada and Totsuka, 1986). This is mainly natural, but in urban environments or near fires, ethene from incomplete combustion can dominate. Sawada and Totsuka (1986) used measurements of ethene emissions

25   per unit biomass to derive a global source of 26.2 Tg yr^{-1} from natural emissions and 9.2 Tg yr^{-1} from anthropogenic emissions, giving a total of 35.4 Tg yr^{-1}, which ranges from 18-45 Tg yr^{-1}. Goldstein et al. (1996) measured ethene emissions from Harvard Forest, Massachusetts, and found that they were linearly correlated with levels of photosynthetically active radiation (PAR), indicating a photosynthetic source. Based on this, they estimated that at Harvard Forest biogenic

30   emissions of ethene correspond to approximately 50% of anthropogenic sources. Using these fluxes, and the ecosystem areas tabulated by Sawada and Totsuka (1986), a global biogenic

source for ethene of 21 Tg yr^{-1} was calculated. This value is similar to the estimates of Hough (1991). The ethene fluxes listed by Poisson et al. (2000), however, are only 11.8 Tg yr^{-1}, while those of Muller and Brasseur (1995) are only 5 Tg yr^{-1}. Abeles et al. (1992) estimate a Terrestrial

35   biogenic source of 16.6 Tg yr^{-1} and an anthropogenic source of 9.2 Tg yr^{-1}. Combustion of fossil fuels amounts to only 21% of these anthropogenic emissions globally, but in urban areas this can be the major source.

There have been previous measurements of ethene by in situ techniques and also by remote sensing. These will be discussed later in the context of comparisons with results from the

40   JPL MkIV interferometer, an infrared Fourier transform spectrometer that uses the sun as a source. We report here long-term remote sensing measurements of C_2H_4 in the lower troposphere, where the vast majority of C_2H_4 resides, by ground-based MkIV observations. We also present MkIV balloon measurements of C_2H_4 in the upper troposphere.

2 Methods

45   ### 2.1 MkIV Instrument

The MkIV Fourier Transform Spectrometer (FTS) is a double-passed FTIR spectrometer designed and built at the Jet Propulsion Laboratory (JPL) in 1984 for atmospheric observations (Toon, 1991). It covers the entire 650-5650 cm^{-1} region simultaneously with two detectors: a HgCdTe photoconductor covering 650-1800 cm^{-1} and an InSb photodiode covering 1800-5650

50   cm^{-1}. The MkIV instrument has flown 24 balloon flights since 1989. It has also flown on over 40 flights of the NASA DC-8 aircraft as part of various campaigns during 1987 to 1992 studying high-latitude ozone loss. MkIV has also made 1132 days of ground-based observations since 1985 from a dozen different sites, from Antarctica to the Arctic, from sea-level to 3.8 km altitude. Details of the ground-based measurements and sites can be found at:

55   http://mark4sun.jpl.nasa.gov/ground.html. MkIV observations have been extensively compared with satellite remote sounders (e.g. Velazco et al., 2009) and with in situ data (e.g., Toon et al., 1999a,b).

2.2 Spectral Analysis

The spectral fitting was performed with the GFIT (Gas Fitting) code, a non-linear least-

60   squares algorithm developed at JPL that scales the atmospheric gas volume mixing ratio (vmr) profiles to fit calculated spectra to those measured. For balloon observations, the atmosphere was

discretized into 100 layers of 1 km thickness. For ground-based observations, 70 layers of 1 km thickness were used. Absorption coefficients were computed line-by-line assuming a Voigt lineshape and using the ATM linelist (Toon, 2014a) for the telluric lines. This is a "greatest hits" compilation, founded on HITRAN, but not always the latest version for every band of every gas. For example, in cases (gases/bands) where the HITRAN 2012 linelist (Rothman et al., 2012) gave poorer fits than HITRAN 2008, the earlier version was retained. The C_2H_4 linelist covering the 950 cm^{-1} region containing the ν_7 and ν_8 bands, is described by Rothman et al. (2003). The solar linelist (Toon, 2014b) used in the analysis of the ground-based MkIV spectra was obtained from balloon flights of the MkIV instrument.
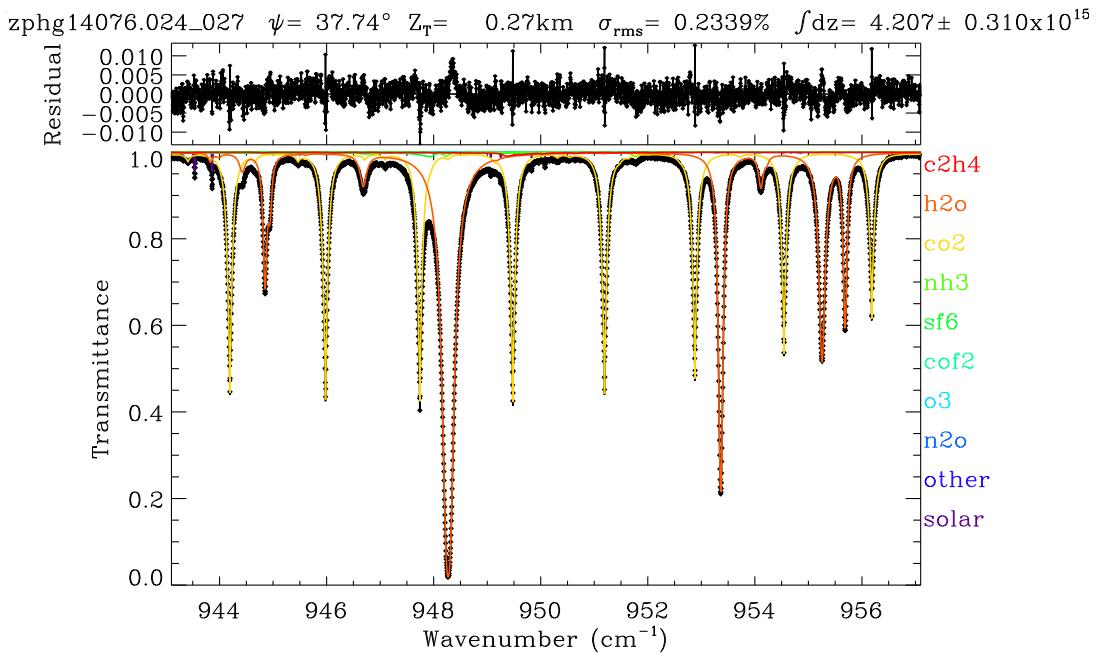
Figure 1. *Example of a fit to a ground-based MkIV spectrum measured from JPL, California, on March 17, 2014 at a solar zenith angle of ψ = 37.7° from a pressure altitude of Z_T = 0.27 km. In the lower panel, black diamond symbols represent the measured spectrum, the black line represents the fitted calculation, and the colored lines represent the contributions of the various absorbing gases; mainly CO_2 (amber) and H_2O (orange). Also fitted are the 0% and 100% signal levels, separate telluric and solar frequency shifts, together with 5 more weakly absorbing gases (NH_3, SF_6, COF_2, O_3, and N_2O). The retrieved C_2H_4 column amount on this day, 4.2×10^{15} molec.cm^{-2}, would represent 2 ppb confined to the lowest 100 mbar (1.5 km) of the atmosphere. The C_2H_4 absorption contribution (red) peaks at 949.35 cm^{-1} with an amplitude of less than 1% and therefore difficult to discern on this plot. The upper panel shows fitting residuals (measured - calculated), peaking at 0.013 (1.3%) with an rms deviation of 0.234%, which are mainly correlated with H_2O and CO_2. The vertical column of C_2H_4 derived from this fit was $4.2 \pm 0.3 \times 10^{15}$ molec.cm^{-2}.*

Sen et al. (1996) provide a more detailed description of the use of the GFIT code for retrieval of vmr profiles from MkIV balloon spectra. GFIT was previously used for the Version 3 analysis (Irion et al., 2003) of spectra measured by the Atmospheric Trace Molecule Occultation Spectrometer (ATMOS), and is currently used for analysis of TCCON spectra (Wunch et al., 2011) and MkIV spectra (Toon, 2016).

We analyzed the strongest infrared absorption feature of ethene: the Q-branch of the ν_7 band (CH_2 wag) at 949 cm^{-1}. This is 7 times stronger than any other feature, including the 3000 cm^{-1} region containing the CH-stretch vibrational modes.

For data acquisition from JPL, the MkIV instrument was indoors with a coelostat mounted to the south wall of the building feeding direct sunlight into the room. Figure 1 shows a fit to the 943-957 cm^{-1} region of one such spectrum. The strongest absorptions are from H_2O lines (orange), one of which is blacked out at 948.25 cm^{-1}. There are also eight CO_2 lines (amber) in this window with depths of 40-60%, one of which sits directly atop the C_2H_4 Q-branch at 949.35 cm^{-1}. These CO_2 lines are temperature sensitive, having ground-state energies in the range 1400 to 1600 cm^{-1}. It is not possible to clearly see the C_2H_4 absorption in Figure 1, and so Figure 2 zooms into the Q-branch region. The lower panel reveals that the peak C_2H_4 absorption is less than 1% deep and strongly overlapped by CO_2. It is also overlapped by absorption from H_2O, SF_6, NH_3, N_2O, and solar OH lines. NH_3 absorption lines exceed 1% in this window on this particular day but do not overlap the strongest part of the C_2H_4 Q-branch. The SF_6 ν_3 Q-branch at 947.9 cm^{-1} also exceeds 1% but fortunately does not overlap the C_2H_4 Q-branch. The SF_6 R-branch, however, underlies the C_2H_4 Q-branch with about 0.3% absorption depth. The upper panel shows the same spectrum fitted without any C_2H_4 absorption. This causes a ~0.5% dip in the residuals around 949.35 cm^{-1} and an increase in the overall rms from 0.234 to 0.251%. The 0.5% dip in the residuals is weaker than the 0.9% depth of the C_2H_4 feature in the lower panel because the other fitted gases have adjusted to try to compensate for the missing C_2H_4. Their inability to completely do so supports the attribution of this dip to C_2H_4.

Given the severity of the interference, especially the directly-overlying 60%-deep CO_2 line, we were at first skeptical that C_2H_4 could be retrieved to a worthwhile accuracy from this window, or any other. But given the good quality of the spectral fits, and the small reported uncertainties, we nevertheless went ahead and analyzed the entire MkIV ground-based spectral dataset, consisting of 4379 spectra acquired on 1208 different days over the past 30 years.

120

14076.024_027 $\psi = 37.74°$ $Z_T = 0.27$km $\sigma_{rms} = 0.2339\%$ $\int dz = 4.207 \pm 0.3$
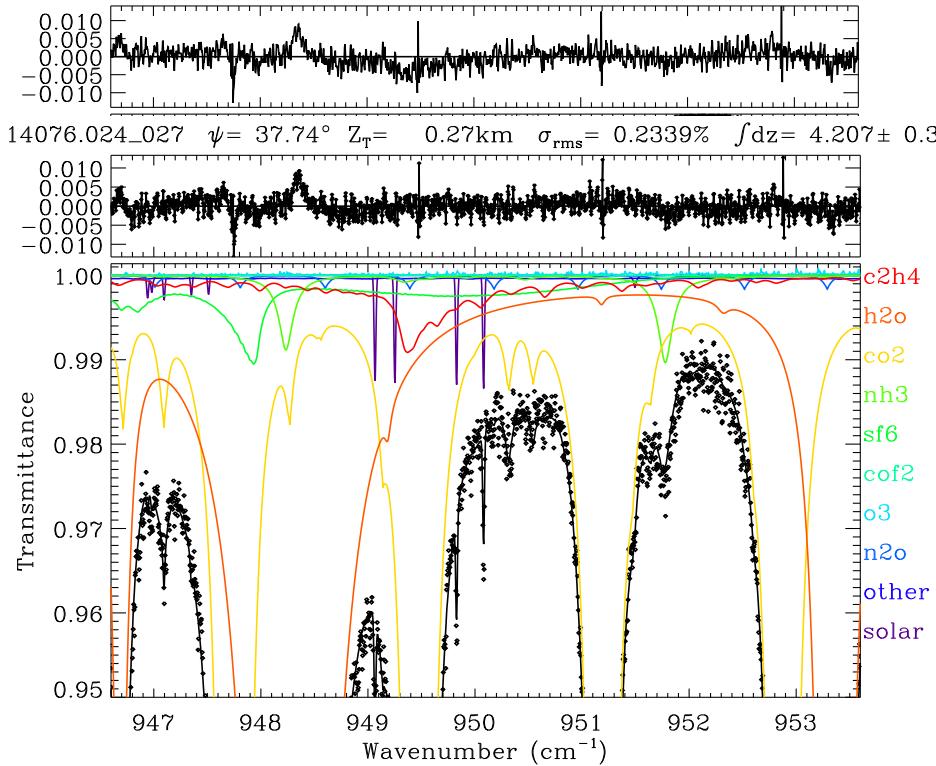
Figure 2. *Lower and middle panels are as described in Figure 1, but zoomed in to reveal more detail of the C_2H_4 Q-branch (red) whose absorption peaks at 949.35 cm^{-1}. The top panel shows residuals from a fit that omitted C_2H_4. This causes a discernable 0.5% dip in the residuals around 949.35 cm^{-1} and a worsening of the RMS spectral fits from 0.234% to 0.251%.*

125

Figure 3 shows the averaging kernel and a priori profile pertaining to the C_2H_4 retrieval illustrated in Figures 1 and 2. The kernel represents the change in the total retrieved column due to the addition of one C_2H_4 molecule.cm^{-2} at a particular altitude. In a perfect column retrieval,

130   the kernel would be 1.0 at all altitudes, but in reality the retrieval is more sensitive to C_2H_4 at high altitudes than near the surface, as is typical for a profile-scaling retrieval of a weakly absorbing gas. The a priori vmr profile has a value of 500 ppt at the surface, dropping rapidly to 10 ppt by 5 km altitude. An even larger fractional drop, from 10 to 0.5 ppt occurs in the lower stratosphere between 15 and 21 km. The slight kink in the averaging kernel (solid line) over this same altitude

135   range is due to this large drop in vmr. Since 99% of the C_2H_4 lies in the troposphere, the stratospheric portion of the averaging kernel is of academic interest only for total column retrievals.
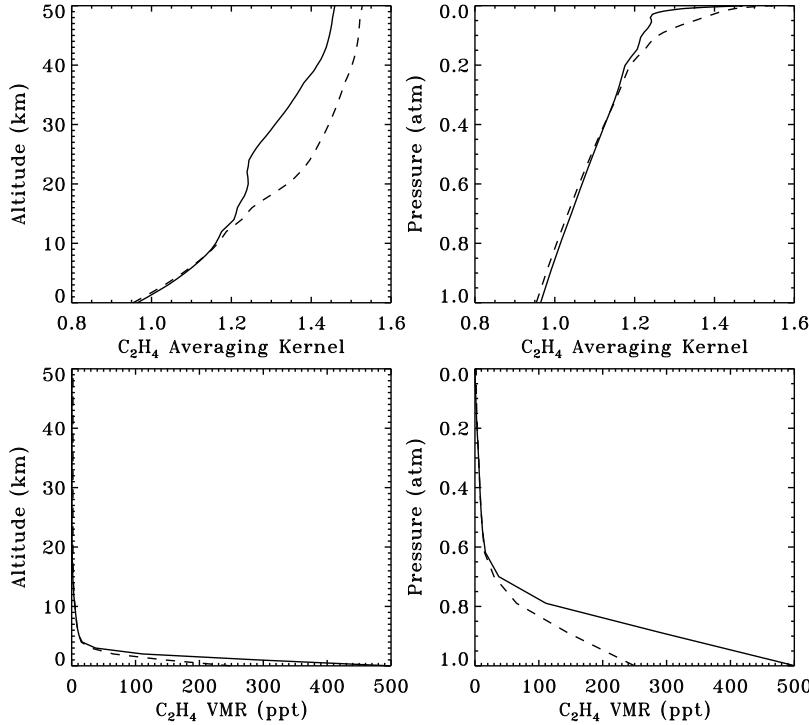
140   *Figure 3. Averaging kernels (upper panels) and a priori volume mixing ratio (vmr) profiles (lower panels) pertaining to the ground-based C_2H_4 retrieval illustrated in Figures 1 and 2. In the left panels quantities are plotted versus altitude. In the right panels, the same data are plotted versus atmospheric pressure. The solid line is the actual profile used. The dashed line is a vmr profile with a less dramatic decrease with altitude: the C_2H_4 vmr below 4 km has been*
145   *halved, with similar amounts in the upper troposphere, and more in the stratosphere. The resulting change in the retrieved total column is only 2%, with the dashed profile giving the smaller columns.*

An important uncertainty in the retrieved column amounts is likely to be the smoothing
150   error, which represents the effect of error in the shape of the a priori vmr profile. If the averaging kernel were perfect (i.e., 1.0 at all altitudes) this wouldn't matter, but in fact the C_2H_4 kernels vary from 0.96 at the ground to 1.4 at 40 km altitude. To investigate the sensitivity of the retrieved column to the assumed a priori profile, we also performed retrievals with a different a priori vmr profile in which the C_2H_4 vmr profile had been halved in the 0-4 km altitude range and increased
155   in the stratosphere, as depicted by the dashed line in Figure 3. The resulting change in the retrieved C_2H_4 column was less than 2% with no discernable change to the rms fitting residuals, which are dominated by the interfering gases. This small C_2H_4 column perturbation is a result of the averaging kernel being close to 1.0 at the altitudes with the largest a priori vmr errors (0 to 3 km). Note that only errors in the ***shape*** of the a priori vmr profile affect the retrieved columns in
160   a profile scaling retrieval.

3 Results

3.1 Ground-based MkIV Retrievals

        Figure 4 shows the retrieved MkIV ground-based C_2H_4 columns from a dozen different observation sites, whose key attributes (e.g. latitude, longitude, altitude, observations, observation days) are presented in the tables of SI.1 and SI.2. The plot is color-coded by the pressure altitude of the site. This was preferred over geometric altitude to prevent all the points from a given site piling up at exactly the same x-value. The pressure altitude varies by up to ±1.5% at the high altitude sites, which is equivalent to ±0.2 km. Only points with C_2H_4 uncertainties $<1x10^{15}$ molecules.cm^{-2} were included in the plot, representing 95.7% of the total data volume. One day (out of 258) at Barcroft (3.8 km altitude) was omitted from the plotted data because it had abnormally high C_2H_4, as well as other short-lived gases -- clearly a local pollution event.
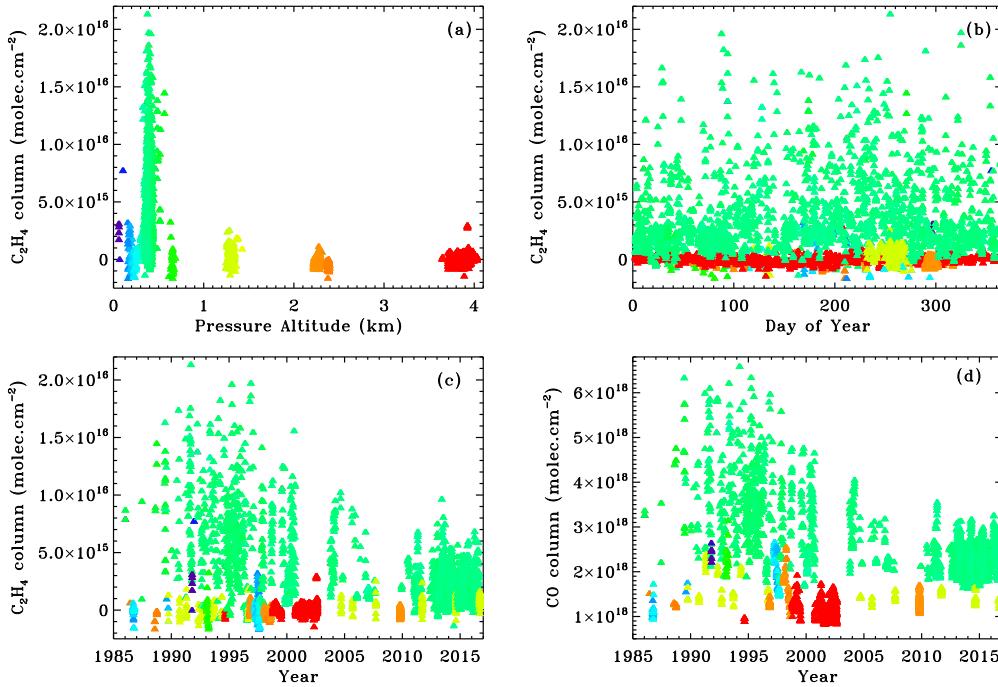
Figure 4. *MkIV column C_2H_4 amounts retrieved from 12 different sites, color-coded by pressure altitude. Significant C_2H_4 amounts are only found at the urban sites: JPL at 0.35 km altitude (green) and Mountain View at 0.01 km altitude (purple). Panel (b) reveals little seasonal variation in C_2H_4. Panel (c) shows a factor 3 decline in C_2H_4 in Pasadena over the past 25 years. Panel (d) shows that the CO columns also decreased since 1990, but never come close to zero.*

        At all sites above 0.5 km altitude there is essentially no measurable C_2H_4. The Table Mountain Facility (TMF) site at 2.3 km altitude (orange) is only 25 km from the most polluted part of the Los Angeles basin, yet no measurable C_2H_4 was recorded there in 45 observation days,

despite the good measurement accuracy at this site (see Figure SI.3). This is probably a result of TMF always being above the PBL (Planetary Boundary Layer), in which urban pollution is trapped, at least on the autumn and winter days when MkIV made measurements at TMF. The high-latitude sites at Fairbanks, Esrange, and McMurdo also have no measurable C_2H_4, as do rural, mid-latitude sites (e.g., Ft. Sumner, NM). The only sites where MkIV has ever detected C_2H_4 are JPL/Pasadena (0.4 km; green) and Mountain View (0.01 km, purple). These sites are part of major conurbations: Pasadena adjoins Los Angeles; Mountain View adjoins San Jose, California.

The main limitation to the accuracy of C_2H_4 measurements by the solar absorption technique is the ability to accurately account for the absorption from CO_2, H_2O, and SF_6, which overlap the Q-branch. The first two gases, in particular, being much stronger absorbers than the C_2H_4, have the potential to drastically perturb the C_2H_4 retrieval. For example, an error in the assumed H_2O vmr vertical profile, and hence the shape of the H_2O absorption line, will have a large effect on retrieved C_2H_4. And since the overlapping CO_2 lines are so T-sensitive (~2%/K), a small error in the assumed tropospheric temperature would greatly influence the C_2H_4 retrieval. Errors in the spectroscopy of H_2O and CO_2 will also strongly affect C_2H_4 retrievals. Figure SI.3 shows the C_2H_4 retrieval uncertainties, estimated by solving the matrix equation that relates the jacobians of the various retrieved quantities to the spectral residuals. The uncertainties are the square root of the diagonal elements of the resulting covariance matrix. The same data are plotted versus year, solar zenith angle and site altitude. From JPL the measurement uncertainty is about 0.5×10^{15} molec.cm^{-2}. At higher solar zenith angles (airmasses) the uncertainty decreases as the C_2H_4 absorption deepens. At higher altitudes the uncertainty decreases as the interfering absorptions shrink faster than that of C_2H_4. There has been no significant change in the C_2H_4 retrieval uncertainty over the 30-year measurement period. We note that the measurements made from McMurdo Antarctica in Sep/Oct 1986 have very small uncertainties, due to their high airmass and the extremely small H_2O absorption. The plotted uncertainties represent a single observation representing a 10-15 minute integration period. 95.7% of the C_2H_4 observations have uncertainties $< 1.0 \times 10^{15}$ molec.cm^{-2}.

At JPL the C_2H_4 column is highly variable. JPL is located at the northern edge of the Los Angeles conurbation, and so when winds are from the Northern sector, or strong from the ocean, pollution levels are much smaller than during stagnant conditions. This is seen in the large range of retrieved C_2H_4 values observed at JPL throughout the year. A notable feature of the MkIV C_2H_4 data (Figure 4c) is the factor 3 drop over the past 25 years. In the 1990's C_2H_4 often topped 16×10^{15} molec.cm^{-2}, but since 2010 a column exceeding 8×10^{15} has only been observed once.

Figure 4d shows the CO time series, which exhibits a substantial decline since the 1990's, although not as dramatic as that of C_2H_4 since CO never falls below 1.5×10^{18} molec.cm^{-2} at JPL, even under the cleanest conditions, due to its non-zero background concentration.
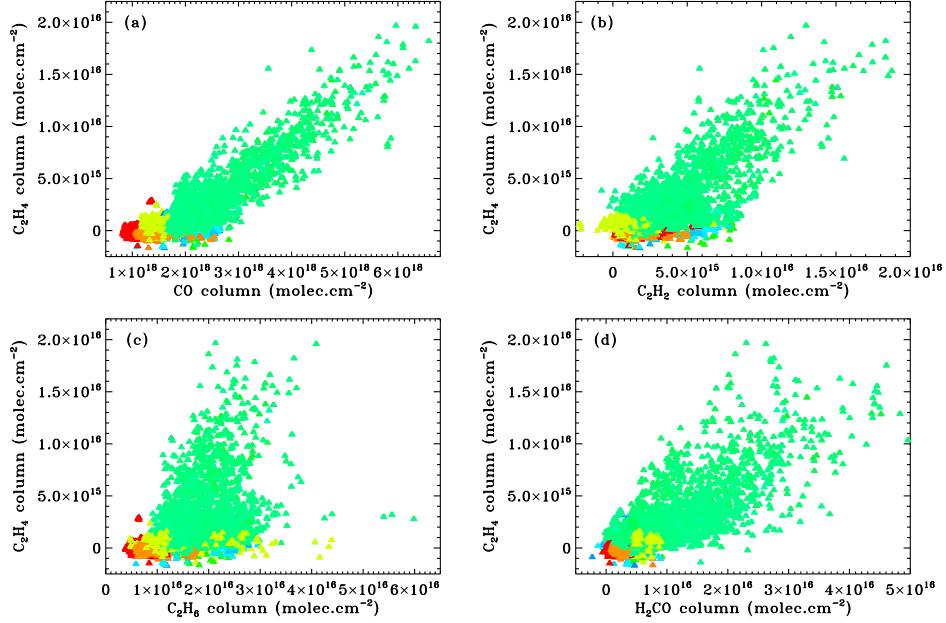
Line 220

Figure 5. *Relationships between C_2H_4 and four other gases: (a)=CO; (b)=C_2H_2, (c)=C_2H_6, and (d)=H_2CO. Points color-coded by altitude, as in Figure 4.*

Figure 5 shows the relationships between C_2H_4 and four other gases: CO, C_2H_2, C_2H_6, and H_2CO. Figure 5a reveals a compact, linear, relationship between C_2H_4 and CO at JPL (green

Line 225

points) suggesting a common local source for both. Figures 5b/c/d show that C_2H_4 is clearly related to the other gases, but not as strongly as with CO. This is likely due to them having other sources, for example, C_2H_6 also comes from natural gas leaks, causing the bifurcated appearance of panel 5c. Since these trace gases are much less abundant than CO, their measurements are noisier, which also degrades the compactness of the relationship.

Line 230

Figure 6 plots the gas column relationships for the JPL data only, color-coded by year to help reveal the long-term changes. The decreases in the CO, C_2H_2, C_2H_4 and H_2CO since the 1990's are evident by the lack of red points in the upper right of the panels plotting these gases. C_2H_6 has not decreased significantly as is evident from the third row of panels, which shows that the 2015 column abundances (red) span similar values to those measured in 1990 (blue). In fact,

Line 235

on November 10, 2015, we observed a factor 2-3 enhancement of the C_2H_6 column as a result of JPL being directly downwind of the Aliso Canyon natural gas leak on that day (Conley et al., 2016). Although this event was associated with a 2.5% enhancement of column CH_4 (not shown

here), there were no enhancements of CO, C_2H_2, C_2H_4, so these particular C_2H_6 points (red) in the third row of Figure 6 protrude upwards from the main clusters. Since C_2H_6 has failed to decrease over the measurement period, unlike the other gases, the C_2H_6-Gas relationships all show a bifurcation, with the later data (red) showing steeper gradients (more C_2H_6).
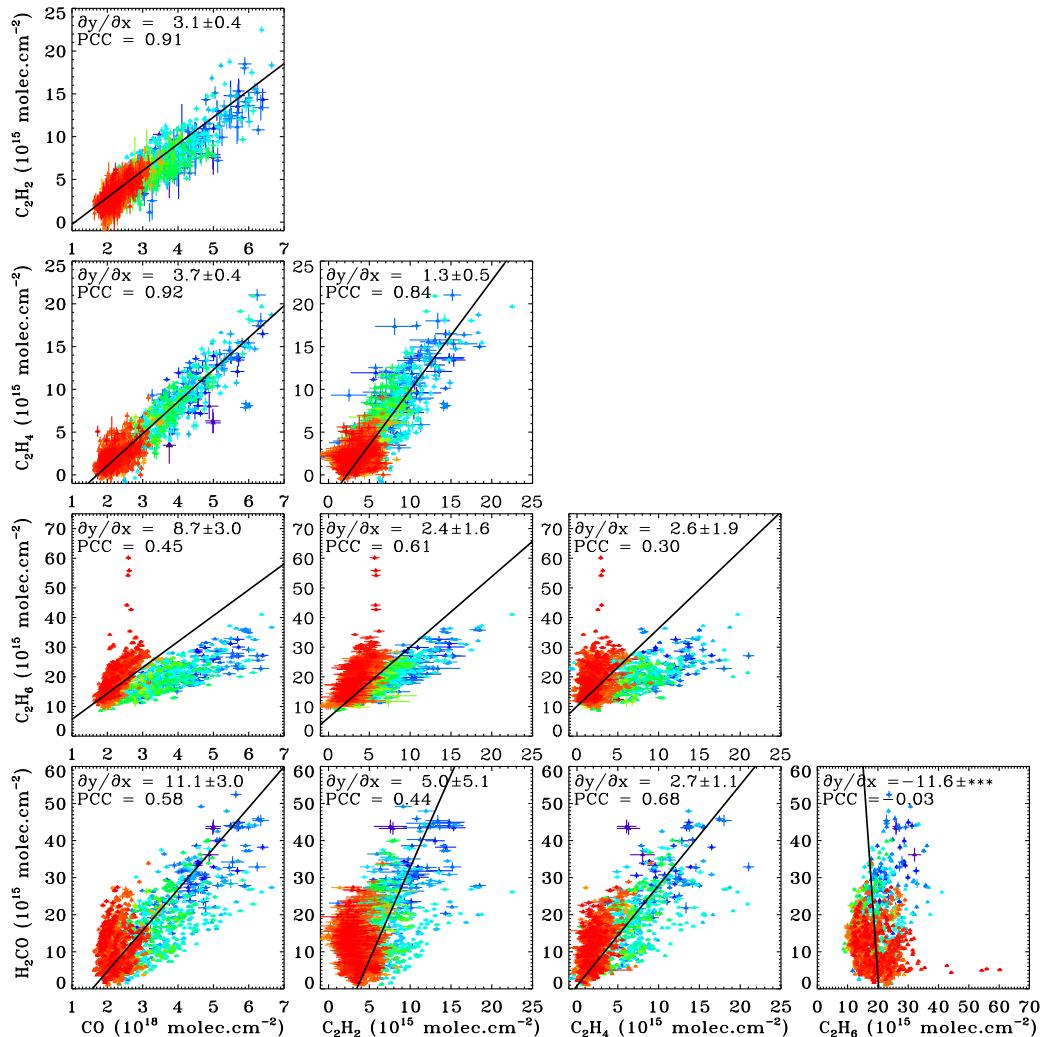
Figure 6. *Relationships between MkIV vertical column abundances of various gases measured from JPL only, color-coded by year (blue = 1990; green = 2000; orange = 2010; red = 2015). The black line in each panel is the best-fit straight line through the data (not constrained to pass through the origin). The gradient of the fitted straight line (∂y/∂x) and the Pearson Correlation Coefficient (PCC) are written at the top of each panel. Panels on the same row all have the same y-axis, avoiding having to repeat the y-annotation. Panels in the same column have the same x-axis, avoiding repeating the x-annotation. Each panel contains 1689 to 1724 observations, representing over 98% of the available JPL data. Note that the CO abundances have been divided by 1000 to bring them closer to the other gases. Thus the Gas:CO gradients are in units of ppt/ppb, whereas the gradients of the non-CO gases are in ppt/ppt. In the first column, the gradients could be termed "emission ratios".*

255   A straight line was fitted through the data in each panel of Figure 6, allowing a gradient and an offset to be computed. The values of the gradients ($\partial y/\partial x$) are written into each panel, along with their uncertainties. The overall gradient of the C_2H_4/CO relationship using all JPL data is 3.8±0.4 ppt/ppb, but the post-2010 JPL data have a gradient of only 2.8±0.4 ppt/ppb. Baker et al. (2008) measured C_2H_4/CO emission ratios of 5.7 ppt/ppb in Los Angeles from whole

260   air canister samples acquired between 1999 and 2005, which is close to their average of all US cities, 4.1 ppt/ppb. Over this same time period the MkIV JPL data reports 3.9±0.7 ppt/ppb, the larger uncertainty reflecting the relatively few observations from JPL over this period. Warneke et al. (2007) report a C_2H_4/CO emissions ratio of 4.9 ppt/ppb in Los Angeles in 2002, measured by aircraft canister samples. Warneke et al. (2012) report decreases of 6-8% yr^{-1} in C_2H_4 and CO

265   over Los Angeles between 2002 and 2010, but little change in the C_2H_4/CO emission ratio, which remained at 5-6 ppt/ppb.

        Figure 6 also includes the Pearson Correlation Coefficients (PCC) of the JPL-only gas relationships. The highest values are between CO and C_2H_2 (0.90) and CO and C_2H_4 (0.92). The PCC between C_2H_2 and C_2H_4 is only 0.84, probably reflecting the fact that C_2H_2 and C_2H_4 are

270   much more difficult to measure (i.e., noisier) than CO. The worst correlation is between C_2H_6 and H_2CO (-0.04).

        To see whether the ground-based MkIV C_2H_4 measured in Pasadena was correlated with the airmass origin, we performed HYSPLIT back-trajectories, and computed the amount of time that airmasses arriving 500 m above JPL had spent over the highly populated areas of Los

275   Angeles conurbation. When column C_2H_4 was plotted versus this time-over-conurbation, the correlation was very poor. Column CO also had a poor correlation. The fact that the C_2H_4 correlates well with CO tends to discount the possibility that the C_2H_4 measurements are wrong, since the CO measurements are very easy. So this implies that the trajectories are not sufficiently accurate. We point out that JPL is located at the foot of the San Gabriel mountains, which rise

280   over 1 km above JPL over a horizontal distance of less than 5 km. This extreme topography might give rise to complexities in the wind fields that might be inadequately represented in the EDAS 40 km-resolution model. Although higher resolution models (e.g. NAM 12km) are available for doing HYSPLIT trajectories, these cover only the past decade, whereas the JPL MkIV measurements go back more than 30 years.

3.2 MkIV Balloon Profiles

We also looked for ethene in MkIV balloon spectra using exactly the same window, spectroscopy and fitting software (GFIT) as used for MkIV ground-based measurements. The advantage of the balloon spectra is that the airmass is much larger and the solar and instrumental features are removed from the occultation spectra by ratioing them against a high-Sun spectrum taken at noon from float altitude.

Figure 7 shows a spectral fit to the MkIV balloon spectrum at 6.1 km tangent altitude measured above Esrange Sweden in Dec 1999. The peak C_2H_4 absorption at 949.35 cm^{-1} is about 6% deep, although this falls beneath a saturated CO_2 line. The information about C_2H_4 at this and lower altitudes therefore comes from adjacent weaker features. At higher altitudes (not shown), where the CO_2 lines are weaker and narrower, the C_2H_4 information comes mainly from the 949.35 cm^{-1} Q-branch.
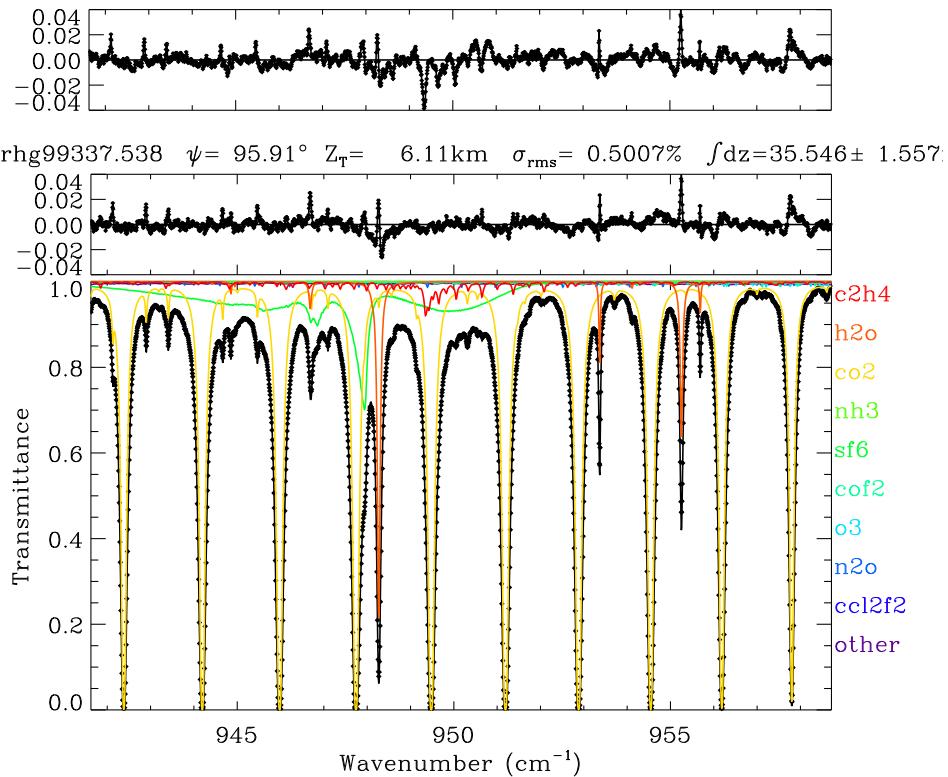
Figure 7. *Lower panel shows a fit to a MkIV balloon spectrum with strong C_2H_4 absorption measured at 6.1 km tangent altitude. The C_2H_4 absorption is denoted by the red line. Its Q-branch is seen at 949.35 cm^{-1} reaching 6% in depth in this particular spectrum. In addition to C_2H_4, other gases were adjusted including H_2O, CO_2, O_3, SF_6, COF_2, N_2O, NH_3, and CCl_2F_2. CH_3OH was included in the calculation but not adjusted. Middle panel shows residuals (measured minus calculated), which are mainly due to H_2O. Upper panel shows residuals after omitting C_2H_4 from the calculation, which causes a large dip in the residuals at 949.35 cm^{-1} and increases the overall rms residual from 0.50% to 0.63%.*

Figure 8 shows 30 balloon profiles of C_2H_4 from 23 flights, color-coded according to date. The C_2H_4 vmr retrieved from the December 1999 flight (green) was 65±6 ppt at 6 km, decreasing to 14±4 at 7 km, and undetectable above. The remaining balloon flights indicate a 10 ppt upper limit for C_2H_4 in the free troposphere and 15 ppt in the stratosphere. Of course, these balloon flights were generally launched under calm, anti-cyclonic, clear-sky conditions, which tend to preclude transport of PBL pollutants up to the free troposphere. So there may be an inherent sampling bias in the MkIV balloon measurements that leads to low C_2H_4.

PBL altitudes (0-3 km) are inaccessible from balloon due to the high aerosol content making the long limb path opaque (although they can be probed from the ground). So the balloon measurements are not inconsistent with C_2H_4 existing in measurable quantities in the polluted PBL, as implied by ground-based measurements. The typical 1-3 day lifetime of C_2H_4 at mid- and low-latitudes implies that it will only be measureable in the free troposphere soon after rapid uplift.
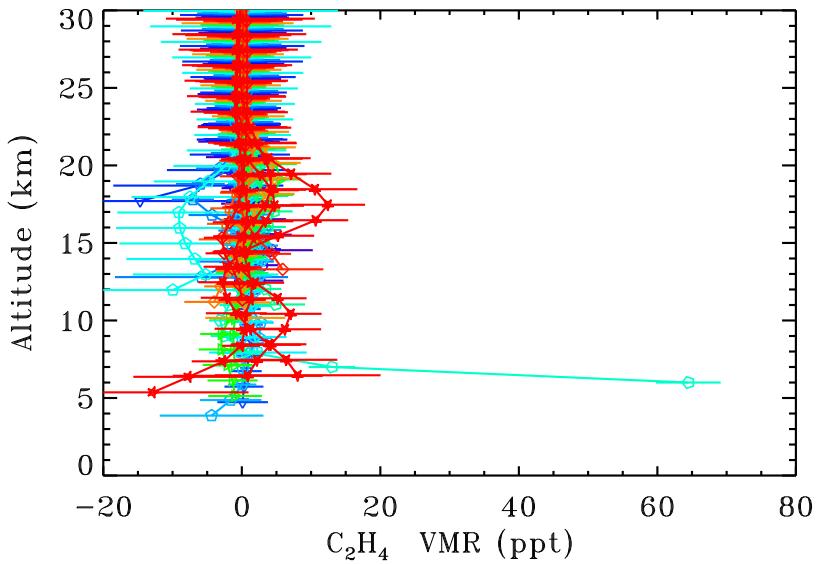
Figure 8. *MkIV C_2H_4 profiles from 24 balloon flights color-coded by year (purple = 1989; green=2000; red = 2014). Altitude offsets of up to 0.4 km have been applied for clarity, to prevent the error bars from over-writing each other at each integer altitude. In only one flight, launched in Dec 1999 from Esrange, Sweden, was a significant amount of C_2H_4 measured (green points at 6-7 km altitude). In other flights there was no detection, with upper limits varying from 10-15 ppt. The increase in uncertainty with altitude above 10 km is due to the C_2H_4 absorption feature weakening in comparison with the spectral noise. Below 10 km the increasing uncertainty is due to the greater interference by H_2O and CO_2. Note that the negative C_2H_4 values are all associated with large uncertainties.*

3.3 Comparison with Remote Sensing Measurements

Paton-Walsh et al. (2005) measured up to 300×10^{15} molec.cm^{-2} of C_2H_4 during fire events in SE Australia in 2001-2003 with aerosol optical depths of up to 5.5 at 500 nm wavelength. From spectra acquired during one of the most intense of these fires (Jan 1, 2002), Rinsland et al. (2005) retrieved a total C_2H_4 column of $380 \pm 20 \times 10^{15}$ through a dense smoke plume and inferred a huge mole fraction of 37 ppb peaking at about 1 km above ground level. This retrieval used information from the shape of the Q-branch feature, which was nearly as deep as the overlapping CO_2 line. These C_2H_4 amounts are 20 times larger than anything seen by MkIV, even from polluted JPL.

Coheur et al. (2007) reported a C_2H_4 vmr of 70 ± 20 ppt at 11.5 km altitude in a biomass-burning plume, observed by the Atmospheric Chemistry Experiment (ACE) (Bernath et al., 2005) off the East coast of Africa. They also show measured C_2H_4 exceeding 100 ppt below 8 km. Simultaneous measurement of elevated C_2H_2, CO, C_2H_6, HCN and HNO_3 confirm their biomass-burning hypothesis.

Herbin et al. (2009) reported zonal-average ethene profiles above 6 km altitude based on global measurements by ACE. Figure 2 of Herbin et al. shows 35°N zonal average vmrs of 40 ppt at 6 km altitude, 30 ppt at 8 km, and 15 ppt at 14 km altitude, with error bars as small as 1 ppt. Herbin et al. (2009) also wrote "We find that a value of 20 ppt is close to the detection threshold at all altitudes in the troposphere". To reconcile these two statements we assume that the 20 ppt detection limit refers to a single occultation whereas the 1 ppt error bar is the result of co-adding hundreds of ACE profiles.

Herbin et al. (2009) also report increasing C_2H_4 with latitude. Although the ACE zonal means agree with the in situ measurements made during the PEM-West and TRACE-P, these campaigns were designed to measure the outflow of Asian pollution and therefore sampled some of the worst pollution on the planet. So one would expect lower values in a zonal average. Based on the total absence of negative values in any of their retrieved vmr profiles, we believe that Herbin et al. performed a log(vmr) retrieval, imposing an implicit positivity constraint. This would have led to a noise-dependent, high bias in their retrieved profiles in places where C_2H_4 was undetectable.

Clerbeaux et al. (2009) reported C_2H_4 column abundances reaching 3×10^{15} molec.cm^{-2} from spectra acquired by the IASI satellite instrument, a nadir-viewing emission sounder. This isolated event occurred on May 2008 over Eastern Asia and was associated with a Siberian fire plume, as confirmed by back-trajectories and co-located enhancements of CH_3OH, HCOOH and NH_3.

More recently, C_2H_4 was detected in boreal fire plumes (Alvarado et al., 2011; Dolan et

365   al., 2016) during the 2008 ARCTAS mission by the Tropospheric Emission Sounder (TES), a

nadir-viewing thermal emission FTS on board the Aura satellite. A strong correlation with CO

was observed. TES's C_2H_4 sensitivity depends strongly on the thermal contrast: the temperature of

the C_2H_4 relative to that of the underlying surface. For plumes in the free troposphere a detection

limit of 2-3 ppb is claimed from a single sounding with a 5 x 8 km footprint.

370

3.4 Comparison with In Situ Measurements

There are a lot of published in situ ethene measurements. Here we intend to discuss only

those that are in some way comparable with MkIV measurements. These include measurements

over the Western US and profiles over the Pacific Ocean in the 30-40ºN latitude range that are

375   upwind of MkIV balloon measurements. Other measurements, e.g., over Europe and mainland

SE Asia, are less relevant, given the 1-3 day lifetime of C_2H_4.

Gaffney et al. (2012) reported surface C_2H_4 over Texas and neighboring states measured

in 2002. They reported a median vmr of 112 ppt, with occasional much larger values of up to 2

ppb, presumably when downwind of local sources. This median value, if present only within a

380   150 mbar-thick PBL, represents a total column of 0.3×10^{15} molec.cm^{-2}, which would be

undetectable in ground-based MkIV measurements, consistent with the non-detection of C_2H_4

from Ft. Sumner, New Mexico (1.2 km)

Lewis et al. (2013) reported airborne in situ measurements of non-methane organic

compounds over SE Canada in summer 2010. The median ethene vmr was 49 ppt with plumes

385   averaging 1848 ppt. Their C_2H_4/CO scatter plot (Figure 2b of Lewis et al.) reveals two distinct

branches. Biomass burning plumes show an emission ratio of 6.97 ppt/ppb, whereas

"local/anthropogenic emissions" show an emission ratio of about 1.3 ppt/ppb. These values

bracket the MkIV value of 3.7±0.5 ppt/ppb obtained from the green points in Figure 5a and all

points of Figure 6 of the current paper.

390   Blake et al. (2003) report mean C_2H_4 profiles from 0 to 12 km during the Feb-Apr 2001

TRACE-P aircraft campaign, during which aircraft based in Hong Kong and Tokyo sampled

outflow from SE Asia. Blake et al. compared these results with those from the similar 1991 and

1994 PEM-West campaigns. Blake et al.'s Figure 11 shows that below 2 km C_2H_4 averaged 100

ppt during TRACE P and 250 ppt during PEM-West. Blake et al.'s Table 1 provides a median

395   C_2H_4 of 30 ppt at 35°N at 2-8 km altitude in the Western Pacific for both TRACE-P and PEM-

West. Below 2 km the vmrs were much larger, especially during PEM-West. Blake et al.'s

Figure 9 shows mean PBL vmrs of 200 ppt during Trace-P and 400 ppt during PEM-West,

rapidly decreasing to 50 ppt by 4 km altitude, 30 ppt by 6 km, and less than 20 ppt above 9 km. Blake et al.'s Figure 2 shows high C_2H_4 in the coastal margins of China, decreasing rapidly by a

400   few hundred km off shore, consistent with the short C_2H_4 lifetime. Since these aircraft campaigns were designed to measure polluted outflow from East Asia, the most polluted region on the planet, their samples cannot be considered representative of a zonal average. Over the mid-Pacific, C_2H_4 amounts were 0-15 ppt at all altitudes during TRACE-P and PEM-West B.

        Sather and Cavender (2016) reported surface in situ measurements of ozone and Volatile

405   Organic Compounds (including ethene) from the cities of Dallas-Ft. Worth, Houston, El Paso, Texas, and from Baton Rouge, Louisiana, over the past 30 years. For ethene the measurements span the late 1990s to 2015, but nevertheless show clear declines by factors of 2-4 during 5-8am on weekdays. The authors attribute this decrease to the impacts of the 1990 amendment to the US Clean Air Act.

410
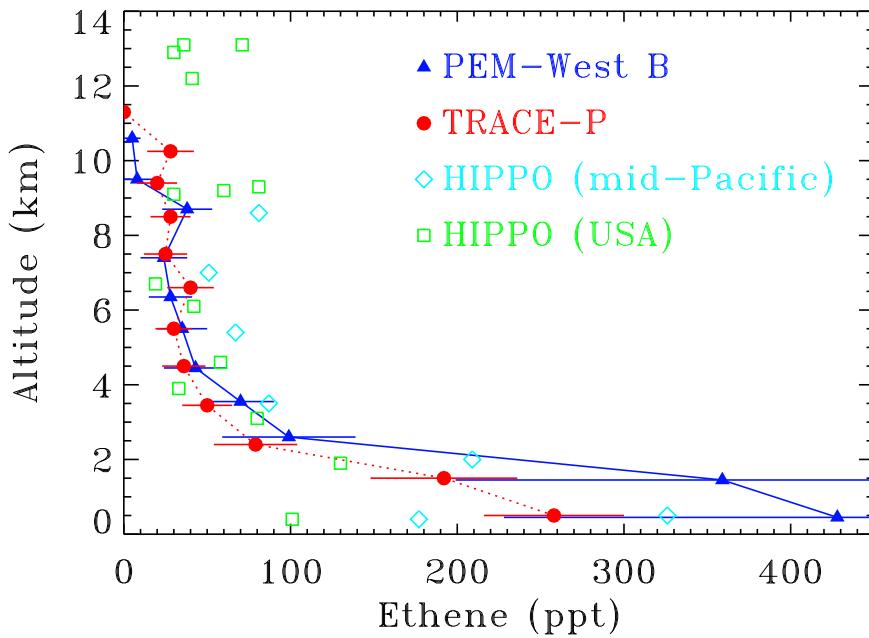
Figure 9. *Aircraft in situ measurements of ethene. HIPPO measurements of C_2H_4 made by the Advanced Whole Air Sampler between 30° to 40°N are shown by cyan diamonds (mid-Pacific) and green squares (Central USA). Also shown are PEM-West B (blue triangles) and TRACE-P (red circles) measurements of C_2H_4 over coastal SE Asia and the Western Pacific (taken from*

415   *Figure 9 of Blake et al. (2003)).*

        Ethene was measured during the HIAPER Pole-to-Pole (HIPPO; Wofsy et al. 2011, 2012) mission by the Advanced Whole Air Sampler. Figure 9 plots the C_2H_4 vmrs measured in the 30-40°N latitude range. Points are color-coded by longitude. The cyan points were measured

420   mid-Pacific in Jan and Dec 2009, Apr 2010, and Jun/Jul 2011. The green points were measured

over the Central/Western USA in Jan and Dec 2009, and Jun/Jul 2011. Profiles from the PEM-West B and TRACE-C aircraft campaigns are plotted in red and blue. Surprisingly, C_2H_4 is larger over the mid-Pacific (blue/purple points) than the USA (red points) at altitudes below 9 km. This is presumably due to Asian pollution being further destroyed while crossing the Eastern

425 Pacific. Above 9 km the C_2H_4 is larger over the USA, presumably due to upward transport of the Asian pollution.

Washenfelder et al. (2011) performed ground-based in situ measurements from Pasadena, California, of several glyoxl precursors in early June 2010, as part of the CalNEX 2010 campaign. An ethene mole fraction of 2.16 ppb was reported. Assuming that this value was

430 present throughout the PBL, extending from the surface at 1000 mbar to the 900 mbar level, then the in situ measurement implies a total C_2H_4 column of 4×10^{15} molec.cm^{-2}, which is consistent with the upper range of values observed by MkIV in 2010. Unfortunately we do not have temporally overlapping measurements, and even if we did JPL is 10 km from the Pasadena site.

Washenfelder et al. (2011) also report a factor 6 drop in C_2H_4 amounts since the

435 September 1993 CalNEX campaign, but note that the 1993 readings occurred during a smog episode, implying higher than normal levels of pollution. This drop is larger than the factor 3 decrease seen in the MkIV column data, but not inconsistent given the sparse statistics together with the large day-to-day variability seen in the MkIV data.

Measurements of ethene from ground level in Mexico City in 1999, 2002, and 2003

440 ranged between 10-60 ppb, with higher levels in the commercial sectors and lower values in residential areas (Altuzar et al., 2001, 2005; Velasco et al., 2007). These are 5-30 times larger than the 2.16 ppb measured by Washenfelder et al. (2011) in Pasadena in 2010.

4 Discussion

The simultaneous reductions in CO and C_2H_4 ground-based column amounts measured

445 from JPL over the past 25 years, and their continued high correlation, suggest a common source: vehicle exhaust. The declines in CO and C_2H_4 are likely a result of improved vehicle emission control systems, mandated by the increasingly stringent requirements imposed by the US Environmental Protection Agency (EPA; e.g., the 1990 Clean Air Act), various state laws, and the California Air Resources Board (CARB, LEV2) over the past decades and stronger

450 enforcement thereof (e.g., smog checks). This view is supported by Bishop and Stedman (2008) who showed that vehicle emissions of hydrocarbons in several US cities including Los Angeles have steadily decreased with vehicle model year since 1986.

C$_2$H$_4$/CO emission ratios measured over JPL by MkIV have decreased over the 30 year record, from 3.7±0.4 ppt/ppb overall to 2.7±0.4 ppt/ppb in recent years. It is not clear what is
455 causing this decrease since many things have changed that might affect C$_2$H$_4$ levels (e.g. regulation of internal combustion engine exhaust, elimination of oil-based paints and lighter fuel, better control of emissions from oil and gas wells).

MkIV balloon measurements have only detected ethane once in 24 flights: in the Arctic in December 1999 at altitudes below 6 km. In all other flights an upper limit of 15 ppt was
460 established for the free troposphere and 10 ppt for the lower stratosphere. These upper limits are substantially smaller than the ACE 35°N zonal mean profiles reported by Herbin et al. (2009), which are possibly biased high when C$_2$H$_4$ amounts are small due to a positivity constraint imposed on the retrievals. Also, a single biomass burning plume with up to 25 ppb of C$_2$H$_4$ has the potential to significantly increase the zonal mean C$_2$H$_4$. For this reason, a zonal median
465 would be a more robust statistic. It is also possible that the MkIV balloon flights under-represent conditions in which PBL pollution is lofted due to their location and the meteorology associated with balloon launches. Herbin et al. (2009) reported an increase of the 6-km ACE C$_2$H$_4$ with latitude in the Northern hemisphere, peaking at 53 ppt at 70°N. This is consistent with the December 1999 MkIV balloon flight from 67°N, which measured 60 ppt at 6 km.
470 MkIV balloon measurements over the Western USA reveal much smaller ethene amounts than in situ aircraft measurements over SE Asia during TRACE-P, PEM-West B, and over the mid-Pacific ocean during HIPPO. With its 1-3 day lifetime, C$_2$H$_4$ decreases substantially during its Eastward journey across the Pacific, which would help reconcile them with the MkIV balloon profiles.
475

5 Summary and Conclusions

A 30-year record of atmospheric C$_2$H$_4$ has been extracted from ground-based FTIR spectra measured by the JPL MkIV instrument. Despite its high sensitivity, MkIV only detects ethene at polluted urban sites (e.g., Pasadena, California). At clean sites visited by MkIV, C$_2$H$_4$
480 was undetectable (less than 10^{15} molec.cm^{-2}). MkIV ground-based measurements are generally consistent with the available surface in situ measurements, although a definitive comparison is difficult due to the large variability of C$_2$H$_4$ and lack of co-incidence.

A large decline in C$_2$H$_4$ has been observed over Pasadena over the past 25 years. This is likely the result of increasingly stringent requirements on vehicle emissions imposed by the US
485 Environmental Protection Agency (e.g., the 1990 Clean Air Act) and the California Air Resources Board (Low Emission Vehicle 2 requirements) over the past decades, together with stronger

enforcement of these regulations (e.g., smog checks). The C_2H_4/CO emissions ratio also appears
to have decreased in recent years.

This work shows that C_2H_4 might in future become a routine product of the NDACC

490   Infra-Red FTS network, at least at sites near large sources. Moreover, since the spectra are saved,
a historical C_2H_4 record may be retro-actively extractable at some of the more polluted sites.

Acknowledgements. This research was performed at the Jet Propulsion Laboratory, California
Institute of Technology, under contract with the National Aeronautics and Space Administration.
495   We thank the Columbia Scientific Balloon Facility (CSBF) who conducted the majority of the
balloon flights. We also thank the CNES Balloon Launch facility who conducted two MkIV
balloon flights from Esrange, Sweden. We thank the Swedish Space Corporation for their
support and our use of their facilities. We thank the HIAPER Pole-to-Pole Observations (HIPPO)
campaign for use of their data. Finally, we acknowledge support from the NASA Upper
500   Atmosphere Research Program. Copyright 2017 California Institute of Technology. Government
sponsorship acknowledged.

References

Abeles, Frederick B., Page W. Morgan and Mikal E. Saltveit, Jr., Ethylene in Plant Biology,
    (Second Edition), ISBN: 978-0-08-091628-6, 1992
505   Altuzar, V., Pacheco, M., Tomas, S.A., Arriaga, J.L., Zelaya-Angel, O., SanchezSinencio, F.,
    2001. Analysis of ethylene concentration in the Mexico City atmosphere by photoacoustic
    spectroscopy. Analytical Sciences 17, 541-543.
Altuzar, V., Tomás, S.A., Zelaya-Angel, O., Sánchez-Sinencio, F., Arriaga, J.L., 2005.
    Atmospheric ethene concentrations in Mexico City: indications of strong diurnal and seasonal
510   dependences. Atmospheric Environment 39, 5215-5225.
Alvarado, M.J., Cady-Pereria, K.E., Xiao, Y., Millet, D.B., Payne, V.H., 2011. Emission ratios
    for ammonia and formic acid and observations of peroxy acetyl nitrate (PAN) and ethylene in
    biomass burning smoke as seen by the tropospheric emission spectrometer (TES).
    Atmosphere, 2, 633-644. http://dx.doi.org/10.3390/atmos2040633.
515   Baker, A. K.; Beyersdorf, A. J.; Doezema, L. A.; Katzenstein, A.; Meinardi, S.; Simpson, I. J.;
    Blake, D. R.; Rowland, F. S., Measurements of nonmethane hydrocarbons in 28 United States
    cities. Atmos. Environ. 2008, 42, 170-182.
Bernath, P.F., McElroy, C.T., Abrams, M.C., Boone, C.D., Butler, M., Camy‐Peyret, C., Carleer,
    M., Clerbaux, C., Coheur, P.F., Colin, R. and DeCola, P., 2005. Atmospheric chemistry
520   experiment (ACE): mission overview. Geophysical Research Letters, 32(15).

Bishop, G. A., and Donald H. Stedman, A Decade of On-road Emissions Measurements, *Environ.
    Sci. Technol.*, 2008, *42* (5), 1651–1656, DOI: 10.1021/es702413b
Blake, N. J., et al. (2003), NMHCs and halocarbons in Asian continental outflow during the
    Transport and Chemical Evolution over the Pacific (TRACE-P) field campaign: Comparison
525   with PEM-West B, J. Geophys. Res., 108(D20), 8806, doi:10.1029/2002JD003367.
Clerbaux, C., Boynard, A., Clarisse, L., George, M., Hadji-Lazaro, J., Herbin, H., Hurtmans, D.,
    Pommier, M., Razavi, A., Turquety, S., Wespes, C., and Coheur, P.-F.: Monitoring of

atmospheric composition using the thermal infrared IASI/MetOp sounder, Atmos. Chem. Phys., 9, 6041-6054, doi:10.5194/acp-9-6041-2009, 2009.

530   Coheur, P-F., et al. "ACE-FTS observation of a young biomass burning plume: first reported measurements of C_2H_4, C_3H_6O, H_2CO and PAN by infrared occultation from space." Atmospheric chemistry and physics 7.20 (2007): 5437-5446

Conley, S., G. Franco, I. Faloona, D. R. Blake, J. Peischl, T. B. Ryerson, Methane emissions from the 2015 Aliso Canyon blowout in Los Angeles, CA, *Science,* 2016, DOI:

535   10.1126/science.aaf2348

Dolan, Payne, Kualwik, and Bowman, Satellite observations of ethylene (C_2H_4) from the Aura Tropospheric Emission Spectrometer: A scoping study, Atmospheric Environment, 141, (2016), 388–393

Gaffney, Jeffrey S., Nancy A. Marley, Donald R. Blake, Baseline measurements of ethene in

540   2002: Implications for increased ethanol use and biomass burning on air quality and ecosystems, Atmospheric Environment 56 (2012), 161-168

Herbin, H., Hurtmans D., Clarisse L., Turquety S., Clerbaux C., Rinsland C. P., Boone C., Bernath P. F., and Coheur P.- F.: Distributions and seasonal variations of tropospheric ethene (C_2H_4) from Atmospheric Chemistry Experiment (ACE-FTS) solar occultation spectra,

545   Geophys. Res. Lett., 36, L04801, doi:10.1029/2008GL036338, 2009.

Hough A.M. (1991). Development of a two-dimensional global troposphere model: Model chemistry. J. Geophys. Res., 96, 7325-7362.

Lewis, A. C., M. J. Evans, J. R. Hopkins, S. Punjabi, K. A. Read, R. M. Purvis, S. J. Andrews, S. J. Moller, L. J. Carpenter, J. D. Lee, A. R. Rickard, P. I. Palmer, and M. Parrington, The

550   influence of biomass burning on the global distribution of selected non-methane organic compounds, Atmos. Chem. Phys., 13, 851–867, 2013, doi:10.5194/acp-13-851-2013

Müller, Jean-François, and Guy Brasseur. "IMAGES: A three-dimensional chemical transport model of the global troposphere." Journal of Geophysical Research: Atmospheres 100.D8 (1995): 16445-16490.

555   Olivella, Santiago, and Albert Solé. "Unimolecular decomposition of β-hydroxyethylperoxy radicals in the HO-initiated oxidation of ethene: A theoretical study." The Journal of Physical Chemistry A 108.52 (2004): 11651-11663.

Paton-Walsh, C., N. B. Jones, S. R. Wilson, V. Haverd, A. Meier, D. W. T. Griffith, and C. P. Rinsland (2005), Measurements of trace gas emissions from Australian forest fires and

560   correlations with coincident measurements of aerosol optical depth, J. Geophys. Res., 110, D24305, doi:10.1029/2005JD006202.

Poisson, N., Kanakidou, M. & Crutzen, P.J., Impact of Non-Methane Hydrocarbons on Tropospheric Chemistry and the Oxidizing Power of the Global Troposphere: 3-Dimensional Modelling Results, Journal of Atmospheric Chemistry (2000) 36: 157.

565   https://doi.org/10.1023/A:100630061654

Irion, F.W., M.R. Gunson, G.C. Toon, A.Y. Chang, A. Eldering, E. Mahieu, G.L. Manney, H.A. Michelsen, E.J. Moyer, M.J. Newchurch, G.B. Osterman, C.P. Rinsland, R.J. Salawitch, B. Sen, Y.L. Yung, and R. Zander, Atmospheric Trace Molecule Spectroscopy (ATMOS) Experiment Version 3 data retrievals, Appl. Opt., 41(33), 6968-6979, 2002.

570   Rothman, L. S., Gordon, I. E., Babikov, Y., Barbe, A., Chris Benner, D., Bernath, P. F., Birk, M., Bizzocchi, L., Boudon, V., Brown, L. R., Campargue, A., Chance, K., Cohen, E. A., Coudert,

L. H., Devi, V. M., Drouin, B. J., Fayt, A., Flaud, J.-M., Gamache, R. R., Harrison, J. J.,
Hartmann, J.-M., Hill, C., Hodges, J. T., Jacquemart, D., Jolly, A., Lamouroux, J., Le Roy, R.
J., Li, G., Long, D. A., Lyulin, O. M., Mackie, C. J., Massie, S. T., Mikhailenko, S., Müller,
H. S. P., Naumenko, O. V., Nikitin, A. V., Orphal, J., Perevalov, V., Perrin, A., Polovtseva,
E. R., Richard, C., Smith, M. A. H., Starikova, E., Sung, K., Tashkun, S., Tennyson, J., Toon,
G. C., Tyuterev, V. I. G., and Wagner, G.: The HITRAN2012 Molecular Spectroscopic
Database, J. Quant. Spectrosc. Ra., 130, 4–50, 2013.

Rothman, L.S., A. Barbe, D. Chris Benner, L.R. Brown, C. Camy-Peyret, M.R. Carleer, K.
Chance, C. Clerbaux, V. Dana, V.M. Devi, A. Fayt, J.-M. Flaud, R.R. Gamache, A.
Goldman, D. Jacquemart, K.W. Jucks, W.J. Lafferty, J.-Y. Mandin, S.T. Massie, V.
Nemtchinov, D.A. Newnham, A. Perrin, C.P. Rinsland, J. Schroeder, K.M. Smith, M.A.H.
Smith, K. Tang, R.A. Toth, J. Vander Auwera, P. Varanasi, K. Yoshino, The HITRAN
molecular spectroscopic database: edition of 2000 including updates through 2001, Journal
of Quantitative Spectroscopy & Radiative Transfer 82 (2003) 5–44

Rinsland, C., Paton-Walsh, C., Jones, N. B., Griffith, D. W., Goldman, A., Wood, S., Chiou, L. &
Meier, A. (2005). High Spectral resolution solar absorption measurements of ethylene (C_2H_4)
in a forest fire smoke plume using HITRAN parameters: Tropospheric vertical profile
retrieval. Journal of Quantitative Spectroscopy and Radiative Transfer, 96 (2), 301-309.

Sather, M.E., K, Cavender. Trends analyses of 30 years of ambient 8 hour ozone and precursor
monitoring data in the South Central U.S.: progress and challenges, *Environ. Sci.: Processes
Impacts*, 2016,18, 819-831

Sawada S., Totsuka T. Natural and anthropogenic sources and fate of atmospheric ethylene.
Atmospheric environment, 20, 821-832, DOI: 10.1016/0004-6981(86)90266-0, 1986

Sen, B., G.C. Toon, J.-F. Blavier, E.L. Fleming, and C.H. Jackman, Balloon-borne observations
of mid-latitude fluorine abundance, J. Geophys. Res., 101(D4), 9045-9054, 1996.

Toon, G.C., The JPL MkIV Interferometer, Opt. Photonics News, 2, 19-21, 1991.

Toon, G. C., J.-F. Blavier, B. Sen, R. J. Salawitch, G. B. Osterman, J. Notholt, M. Rex, C. T.
McElroy, and J. M. Russell III (1999a), Ground-based observations of Arctic O_3 loss during
spring and summer 1997, J. Geophys. Res., 104 (D21), 26497–26510,
doi:10.1029/1999JD900745.

Toon, G.C., J.-F. Blavier, B. Sen, J.J. Margitan, C.R. Webster, R.D. May, D.W. Fahey, R. Gao,
L. Del Negro, M. Proffitt, J. Elkins, P.A. Romashkin, D.F. Hurst, S. Oltmans, E. Atlas, S.
Schauffler, F. Flocke, T.P. Bui, R.M. Stimpfle, G.P. Bonne, P.B. Voss, and R.C. Cohen,
Comparison of MkIV balloon and ER-2 aircraft profiles of atmospheric trace gases, J.
Geophys. Res., 104, 26,779-26,790, 1999b.

Toon, G. C. 2014a. Telluric line list for GGG2014. TCCON data archive, hosted by the Carbon
Dioxide Information Analysis Center, Oak Ridge National Laboratory, U.S.A.
http://dx.doi.org/10.14291/tccon.ggg2014.atm.R0/1221656

Toon, G. C. 2014b. Solar line list for GGG2014. TCCON data archive, hosted by the Carbon
Dioxide Information Analysis Center, Oak Ridge National Laboratory, U.S.A.
http://dx.doi.org/10.14291/tccon.ggg2014.atm.R0/1221658

Toon, G.C., J.-F. Blavier, K. Sung, L.S. Rothman, I. Gordon, HITRAN spectroscopy evaluation
using solar occultation FTIR spectra, J. Quant. Spectrosc. Radiat. Transfer (2016),
http://dx.doi.org/10.1016.j.jqsrt.2016.05.21

Velasco, E., Lamb, B., Westberg, H., Allwine, E., Sosa, G., Arriaga-Colina, J.L., Jobson, B.T., Alexander, M., Prazeller, P., Knighton, W.B., Rogers, T.M., Grutter, M., Herndon, S.C., Kolb, C.E., Zavala, M., de Foy, B., Volkamer, R., Molina, L.T., Molina, M.J., 2007. Distribution, magnitudes, reactivities, ratios and diurnal patterns of volatile organic compounds in the Valley of Mexico during the MCMA 2002 and 2003 field campaigns. Atmospheric Chemistry and Physics 7, 329-353.

Warneke, C.; McKeen, S. A.; De Gouw, J. A.; Goldan, P. D.; Kuster, W. C.; Holloway, J. S.; Williams, E. J.; Lerner, B.; Parrish, D. D.; Trainer, M.; Fehsenfeld, F. C.; Kato, S.; Atlas, E. L.; Baker, A.; Blake, D. R., Determination of urban volatile organic compound emission ratios and comparison with an emissions database. J. Geophys. Res.-Atmos. 2007, 112, D10S47.

Warneke, C., J. A. deGouw, J. S. Holloway, J. Peischl, T. B. Ryerson, E. Atlas, D. Blake, M. Trainer, and D. D. Parrish (2012), Multiyear trends in volatile organic compounds in Los Angeles, California: Five decades of decreasing emissions, J. Geophys. Res., 117, D00V17, doi:10.1029/2012JD017899.

Washenfelder, R. A., et al. (2011), The glyoxal budget and its contribution to organic aerosol for Los Angeles, California, during CalNex 2010, J. Geophys. Res., 116, D00V02, doi:10.1029/2011JD016314.

Wofsy, S. C., THE HIPPO SCIENCE TEAM AND COOPERATING MODELLERS AND SATELLITE TEAMS, HIAPER Pole-to-Pole Observations (HIPPO): fine-grained, global-scale measurements of climatically important atmospheric gases and aerosols, Phil. Trans. R. Soc. A (2011) 369, 2073–2086 doi:10.1098/rsta.2010.0313

Wofsy, S. C., B. C. Daube, R. Jimenez, E. Kort, J. V. Pittman, S. Park, R. Commane, B. Xiang, G. Santoni, D. Jacob, J. Fisher, C. Pickett-Heaps, H. Wang, K. Wecht, Q.-Q. Wang, B. B. Stephens, S. Shertz, A.S. Watt, P. Romashkin, T. Campos, J. Haggerty, W. A. Cooper, D. Rogers, S. Beaton, R. Hendershot, J. W. Elkins, D. W. Fahey, R. S. Gao, F. Moore, S. A. Montzka, J. P. Schwarz, A. E. Perring, D. Hurst, B. R. Miller, C. Sweeney, S. Oltmans, D. Nance, E. Hintsa, G. Dutton, L. A. Watts, J. R. Spackman, K. H. Rosenlof, E. A. Ray, B. Hall, M. A. Zondlo, M. Diao, R. Keeling, J. Bent, E. L. Atlas, R. Lueb, M. J. Mahoney. 2012. HIPPO Merged 10-second Meteorology, Atmospheric Chemistry, Aerosol Data (R_20121129). Carbon Dioxide Information Analysis Center, Oak Ridge National Laboratory, Oak Ridge, Tennessee, U.S.A. http://dx.doi.org/10.3334/CDIAC/hippo_010 (Release 20121129)

Wunch, D., G. C. Toon, J.-F. L. Blavier, R. A. Washenfelder, J. Notholt, B. J. Connor, D. W. T. Griffith, V. Sherlock, and P. O. Wennberg (2011), The total carbon column observing network, Philosophical Transactions of the Royal Society - Series A: Mathematical, Physical and Engineering Sciences, 369(1943), 2087-2112, doi:10.1098/rsta.2010.0240.

Xue, Likun, Tao Wang, Isobel. J. Simpson, Aijun Ding , Jian Gao , Donald. R. Blake , Xuezhong Wang , Wenxing Wanga, Hengchi Lei, Dezhen Jin, Vertical distributions of non-methane hydrocarbons and halocarbons in the lower troposphere over northeast China, Atmospheric Environment 45, (2011), 6501-6509

Supplementary Information

665 ***Table SI.1.*** *Summarizing the twelve observation sites from which the JPL MkIV instrument has made ground-based observations as of the end of 2016, sorted by latitude. For each site, the latitude, longitude, and altitude are listed, together with the type of surrounding terrain, the season, and time of day when observations were typically made. The number of observations (N_{obs}) and observation days (N_{day}) from each site are also provided. JPL has the most*

670 *observation days with 648+5=653, followed by Mt. Barcroft (258), and Ft. Sumner (89).*

Table SI.2. *MkIV ground-based observation days at the 12 different sites, broken down by year. 2001 was the year with the most observations days (101) all from Mt. Barcroft. JPL is the site with the most observation days (653).*

675

Figure SI.3. *C_2H_4 retrieval uncertainties, color-coded by pressure altitude, plotted versus year (top), solar zenith angle (middle), and pressure altitude (bottom). At any given site, ethene uncertainties decrease with solar zenith angle as the absorption features deepen (middle panel). In absolute terms the uncertainties are smallest at the highest altitude sites (lower panel), where*

680 *ethene is virtually never detectable. In fractional terms, ethene uncertainties are smallest at the low altitude polluted sites.*